DOI 10.2478/ama-2024-0020

EXAMINATION OF A MAGNETORHEOLOGICAL DAMPER CONTROL SYSTEM WITH VIBRATION ENERGY HARVESTING

Łukasz JASTRZĘBSKI*, Bogdan SAPIŃSKI**

*Faculty of Mechanical Engineering and Robotics, Department of Process Control,
AGH University of Krakow, Mickiewicza 30 av., Kraków, Poland

lukasz.jastrzebski83@gmail.com, deep@agh.edu.pl

received 30 June 2023, revised 15 September 2023, accepted 17 September 2023

Abstract: The study deals with the experimental examination of a magnetorheological (MR) damper control system with vibration energy harvesting using a specially engineered electronic unit (EU). Unlike a typical MR damper control system, which requires an external energy source, the developed system is powered exclusively by energy extracted from a vibrating structure (mechanical system with one-degree-of freedom) and processed through the EU. The work describes the structure and functions of the EU, presents the test rig and the control algorithm implementation, and discusses the test results of the control system under harmonic kinematic excitations of low frequency range.

Key words: magnetorheological damper, vibration, harvester, electronic unit, control system, algorithm.

1. INTRODUCTION

Research interest on vibration energy harvesting has been growing rapidly. The topic has emerged as a promising solution for regenerative power due to increasing demand for self-powered technologies. Recent studies and developments in techniques for vibration energy harvesting have been widely reported in the literature [e.g. 1–5].

The kinetic energy present in vibrating structures, such as vehicle suspensions, civil structures and others, can provide sustainable power. The energy extracted from these structures by the use of harvesters is converted into usable electrical energy with requirements ranging from large- to small-scale power. The limitation of vibration harvesting techniques is performance of the power output. The harvester is usually designed in such a way that the maximum amount of energy it recovers is obtained at the resonant frequency of the vibrating structure [6, 7]. Moreover, the harvester excited by the structure produces AC power, which must be processed before it can be used with any sensor, actuator or conditioning/control electronics requiring DC power. Most often, a bipolar Graetz bridge rectifier is applied for this purpose, which directly powers the load [8, 9], or a DC–DC voltage converter based on a dedicated integrated circuit [10] or on a microcontroller (μC) [11].

This study concerns the magnetorheological (MR) damper control system with vibration energy harvesting using a newly developed electronic unit (EU). The objective of the research is to examine this system and to demonstrate its applicability for effectively controlling the MR damper employed in a mechanical system with one-degree-of freedom. This is done with the assumption that the level of energy extracted from the structure and converted into electrical energy enables the EU and applied sensors to be powered as well as the MR damper to be controlled [12]. To control the MR damper, we employ a typical sky-hook algorithm whose task is to shape the current in the MR damper coil in such a way that it enables reducing the amplitude of sprung mass vibrations at frequencies that are higher than the resonant frequency [13].

The remainder of this article is structured as follows. Section 2 presents a concept and components of the MR damper control system with vibration energy harvesting. Section 3 describes the test rig. Section 4 concerns control algorithm implementation in the μC. Section 5 presents and discusses the results of tests conducted for the examined control system. The conclusions are drawn in Section 6.

2. CONTROL SYSTEM

2.1. Concept

A general concept of processing of energy extracted from a vibrating structure into usable energy to power a device is illustrated Fig. 1.

The diagram comprises three blocks. The first block concerns conversion of kinetic energy of the vibrating structure into electrical energy using a harvester, whereas the second block refers to power processing using conditioning electronics, which enables AC–DC voltage conversion andthereafter DC–DC voltage regulation. The third block refers to powering the load (current in the electrical circuit of a device). In the present study, the first block is represented by an electromagnetic harvester, the second by the EU and the third by the MR damper.

DOI 10.2478/ama-2024-0020

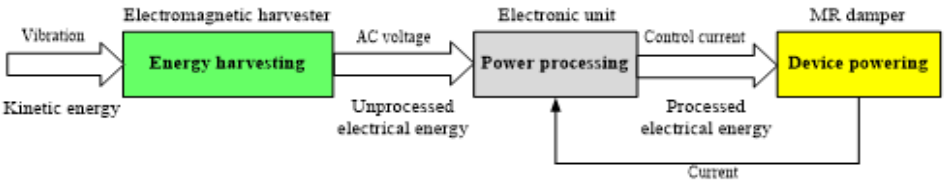

Fig. 1. Processing of the energy extracted from a vibrating structure to power a device

2.2. Components

2.2.1. Electromagnetic harvester

The working principle of the harvester is to use the Faraday's law. The electromotive force induced in the harvester circuit is linked to the product of the flux linkage gradient and the velocity. The harvester is an improved version of the device developed in Sapiński's study [14], and it is further modified as reported in a subsequent study by Sapiński [15]. The structure of the harvester is depicted in Fig. 2a.

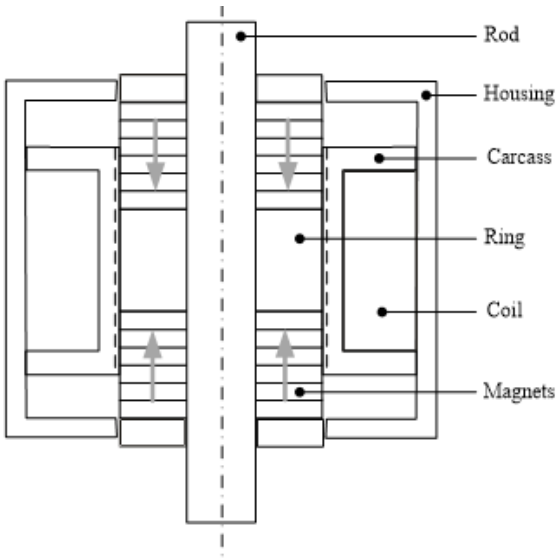

(a)

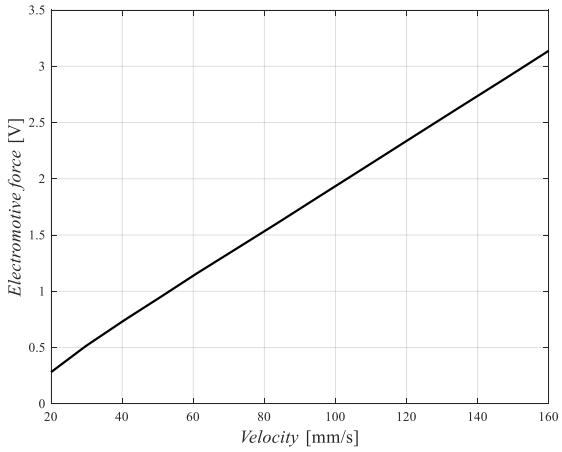

(b)

Fig. 2. Electromagnetic harvester: (a) structure, (b) electromotive force vs. velocity

It consists of a movable non-magnetic rod to which two systems of neodymium-boron magnets (six ring magnets each) are fixed. The systems of magnets face each other with the same poles and are separated by a ferromagnetic ring. The non-moving part of the device includes of a copper foil coil wound on a diamagnetic plastic spool attached to the ferromagnetic housing. The electric constant of the harvester, representing the relationship between the electromotive force induced in the coil and relative velocity of magnets, is equal to 18.5 Vs/m, whereas the resistance and inductance of its coil are, respectively, given as Rh = 0.25 Ω and Lh = 4.78 mH. The relationship between the electromotive force and the relative velocity of the device is provided in Fig. 2b.

2.2.2. EU

The EU is an improved version of the unit described in Kozieł et al.'s study [16]. The unit was developed for the MR damper-based vibration control system with energy harvesting. The diagram depicted in Fig. 3 shows that the EU consists of the following blocks: the rectifier bridge (RB), the driver unit (DU), the low power μC and the internal power supplier (IPS). The most important difference between the present and earlier versions of the unit is that the former enables powering both the μC and the MEMS accelerometers employed in the EU measurement-control system exclusively with energy recovered from structural vibrations. The use of MEMS accelerometers requires increased calculations and operations performed by the μC, which is due to the conversion of acceleration signals into velocity signals resulting from the adopted control algorithm. It should be noted that the EU has the ability to connect an energy storage acting as an additional power source. However, this storage can only be used to power one of the EU units and not the MR damper coil.

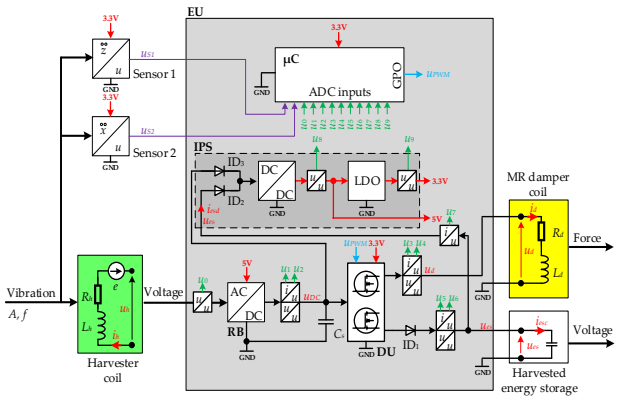

Fig. 3. Electronic unit

DOI 10.2478/ama-2024-0020

The main functions of the EU are:

- conditioning of the voltage generated in the harvester coil uh, its rectification with high efficiency and smoothing and filtration to minimise the pulsation of the rectified voltage uDC;
- production of stable 5 V and 3.3 V voltage sources for power supply of the EU circuits;
- collection of measurement data for the control algorithm and internal diagnostics;
- the capacitor smoothing ripples of voltage uDC in the bridge outlet are neglected;
- accumulation of excess recovered energy in an energy storage that can be used to power the EU when the amount of recovered energy is insufficient.

The RB is responsible for rectifying the AC voltage uh generated by the harvester into DC voltage uDC. The RB consists of a bipolar rectifier (Graetz bridge) built on FET transistors operating as ideal diodes (reducing power losses). An electrolytic capacitor Cs = 62 mF, connected to the RB output, reduces voltage ripple. The voltage uDC supplies both the IPS and the MR damper through the DU. When the RB electronic circuits are powered by a stable voltage of 5 V, it operates with an efficiency >90%, and when the RB is not powered, it rectifies the voltage uh with lower efficiency using Schottky diodes built into the FET transistors.

The IPS converts the voltage uDC to stabilised voltages of 5 V and 3.3 V, required by the RB, DU, µC circuits and the MEMS accelerometers. The voltage uDC is increased to the required level of 5 V by the TPS61200 DC/DC boost converter [17]. The voltage 3.3 V is produced by a linear LDO stabiliser powered by the voltage of 5 V. The IPS can also be supplied from the harvested energy storage with the voltage ues. The IPS turns on when the voltage uDC or ues is >0.7 V and turns off when the voltages uDC and ues are <0.3 V, using the ideal diodes ID2 and ID3.

The DU is responsible for connecting/disconnecting the MR damper coil and the energy storage from the voltage uDC. The unit is built of two identical circuits, each of which consists of a part amplifying the control voltage uPWM and the FET transistor. The conditioning part is used to amplify and adjust the voltage uPWM, which ensures the operation of the FET at full clogging or saturation. The voltage uPWM can take the following states: low (0 V), high (3.3 V) and high impedance (H-Z). The DU can supply energy to only one receiver (MR damper coil or energy storage) at a time. When uPWM = 0 V or is in the H-Z state, the MR damper coil is powered. However, when uPWM = 3.3 V, it is powered from the harvested energy storage. Thus, the MR damper coil is attached to the RB by default when the IPS and µC do not operate (then the control algorithm is not implemented and the uPWM is in the H-Z state). The diode ID1 prevents reverse current flow from harvested energy storage to the RB.

The µC based on the 32-bit STM32L476G µC [18] performs a measurement-control function. It is responsible for the supervision of the conditioning of the harvested energy, the diagnosis of the EU, the production of the control signal uPWM and acquisition of measurement data. Acquisition of measurement data (voltages in the range 0–3.3 V) is carried out using two 12-bit analogue-to-digital converters (ADC1 and ADC2) operating in direct memory access mode. The voltages us1 and us2 from the sensors S1 and S2 corresponding to accelerations $\ddot{z}$ and $\ddot{x}$ are processed by the ADC1 converter, which operates in the 16-fold oversampling mode (filtering the signal by averaging subsequent samples) and the sampling frequency 4 kHz. The ADC2 converter processes input voltages from u0 do u10, enabling the acquisition of, respectively, uh output voltage of the harvester, uDC voltage, iDC current, ud voltage and id current in the MR damper coil, ues voltage and ies current in the harvested energy storage, and supply voltages of 5 V and 3.3 V produced by the IPS. The ADC2 converter was configured to operate at a sampling rate of 16 kHz. To implement the control algorithm for the current id, two hardware timers (TIM16 and TIM15) are used to generate interrupts of 1 ms and 100 µs, respectively.

2.2.3. MR damper

The MR damper is a controllable hydraulic device that dissipates the kinetic energy of a vibrating structure. The amount of energy dissipated depends both on the relative velocity of the piston rod and the cylinder movement, as well as on the current values in the coil that generates the magnetic field in the annular orifice through which the MR fluid flows. In the present study, we use the RD-8040-1 damper of Lord Co. [19], and the structure of the same is as shown in Fig. 4a. The damper features two distinct hysteretic mechanisms of differing natures, mechanical/hydraulic (see force-velocity loops at various current levels in Fig. 4b) and magnetic (resulting from properties of ferromagnetic materials forming the device's electromagnet circuit) [20]. The coil resistance Rd of the RD-8040-1 damper is 5.5 Ω and the coil inductance Ld is 125 mH.

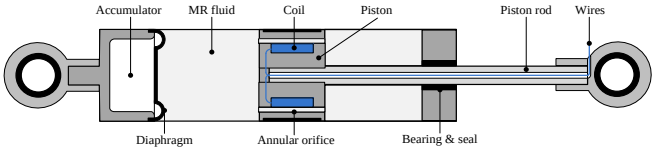

(a)

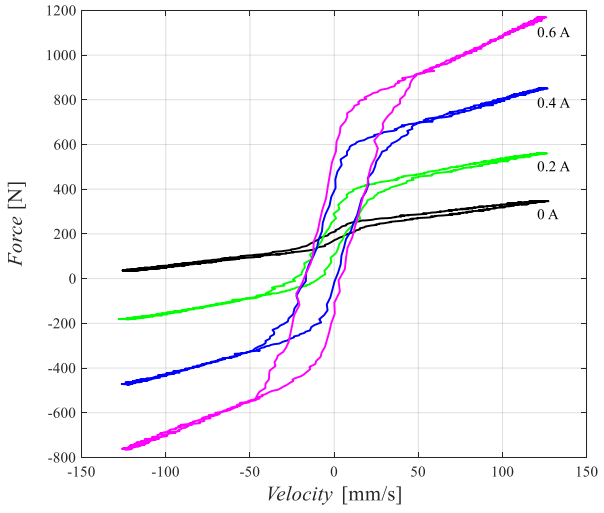

(b)

Fig. 4. Magnetorheological damper: (a) structure, (b) force-velocity loops

DOI 10.2478/ama-2024-0020

3. TEST RIG

The diagram of the test rig for examination of MR damper control with energy harvesting is depicted schematically in Fig. 5. The rig consists of three assemblies of elements: an electrodynamic shaker, a tested vibration control system with energy harvesting implemented in a mechanical system with one-degree-of freedom and an external measurement system. The mechanical system employs: an electromagnetic harvester, an MR damper (RD-8040-1), a sprung mass (mobile steel platform with mass m = 150 kg), a helical compression spring with the stiffness coefficient k = 100,000 N/m, and the EU. The natural frequency of the system, which is a compound of sprung mass, spring, MR damper and harvester, is given as f0 = 4.1 Hz. The external measurement system allows the following quantities to be acquired: shaker plate displacement z, sprung mass displacement x, harvester coil voltage uh and current ih, MR damper coil current id and MR damper force Fd. There needs to be a clear emphasis on the fact that the external measurement system is powered by an external power source. It is responsible only for the acquisition of the above quantities and does not participate in controlling the MR damper. The EU and the S1 and S2 sensors (operating independently of the measurement system) are powered exclusively by energy harvested from vibrations. The harvester force Fh and spring force Fs denoted in Fig. 3 were not measured in the conducted tests.

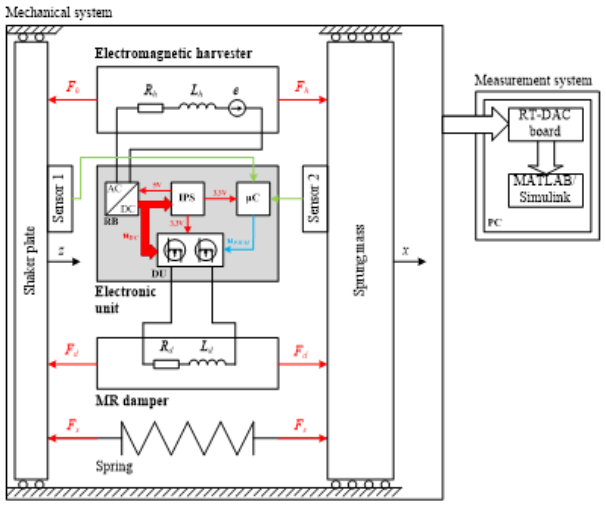

Fig. 5. Test rig

4. CONTROL ALGORITHM IMPLEMENTATION

The algorithms applied to control the MR dampers are discussed in Choi et al.'s study [21]. The control algorithm affects, on the one hand, the complexity of the calculations performed by the μC, and on the other hand, the reduction in the amplitude of the sprung mass vibrations. It should be noted that the low power consumption of the EU requires limiting the clock frequency of the μC. As a result, this reduces the computing power and at the same time increases the time required to perform the necessary numerical calculations. This led us to consider the sky-hook algorithm [22]. Given that the current level in the MR damper coil only affects the amount of energy dissipated, we assumed the sky-hook algorithm which is dedicated to semi-active systems. According to this algorithm, the current ids in the MR damper coil is calculated according to the formula:

$$i_{ds} = \begin{cases} b|\dot{x}| & ;\ \dot{x}(\dot{x}-\dot{z}) > 0 \\ 0 & ;\ \dot{x}(\dot{x}-\dot{z}) \le 0 \end{cases} \quad (1)$$

where the ratio b = 2 A·s/m was determined experimentally.

To obtain a set current value ids, an on-off controller was implemented in the μC determining the control signal uPWM as follows [23]:

$$u_{PWM} = \begin{cases} 3.3\ \text{V} ;\ i_d < i_{ds} \\ 0\ \text{V} ;\ i_d \ge i_{ds} \end{cases} \quad (2)$$

The EU has been engineered to work with two MEMS accelerometers (S1 and S2) of type ADXL335 [24] with an analogue output measuring range of ±3.6 g and an analogue output sensitivity of 300 mV / g (30.58 mV·s2· m–1). The type of these accelerometers was decided based on their very low power consumption (about 1.5 mW), which allows them to be powered by the EU (3.3 V voltage from the IPS). Since accelerometers S1 and S2 measure acceleration ẍ and z̈, it is necessary for them to be converted into the corresponding velocity signals ẋ and ż by the μC. There is a close mathematical relationship between acceleration and velocity that allows the reconstruction of the velocity signal based on the measured acceleration through integration [25]. However, due to the unknown initial velocity of a vibrating structure, direct integration is mostly impractical due to errors in initial values and background or sensor noise [26]. A nonzero constant velocity value added to the actual velocity of the sprung mass as a result of numerical integration causes the current value ids controlling the MR damper to be calculated incorrectly by the sky-hook algorithm. Therefore, the elimination of the integral constant becomes a key issue. The literature describes various methods for processing acceleration to velocity to reduce conversion errors. They can be divided into two categories of numerical integration, in the frequency domain and in the time domain. The frequency method is to convert the acceleration signal to the frequency domain using Fourier transforms, and then determine the velocity using the transfer functions and the inverse Fourier transform [27–29]. The key issue in the method of time domain integration is to remove the constant component resulting from numerical integration [29–31]. In the present study, we used a simplified method of numerical integration in the time domain, assuming that only acceleration harmonics with a frequency of 2–10 Hz would be processed.

This method of velocity calculation $\dot{x}_c(t)$ from acceleration takes place in three steps (see Fig. 6).

Step 1.

- Remove the constant component from the measured acceleration;
- determine the frequency f and the period T of acceleration using detection of zero-crossings of the signal $\ddot{x}(t)$; and
- determine the velocity $\dot{x}_i(t)$ by integration of acceleration using the rectangle method according to the formula:

$$\dot{x}_i(t) = \int_0^t \ddot{x}(t)dt \approx \sum_{j=1}^{N} \ddot{x}_j \cdot T_{as} \quad (3)$$

where Tas = 1/fas is the sampling period of the acceleration signal by μC (fas = 1 kHz).

DOI 10.2478/ama-2024-0020

Step 2.

– Calculate the average velocity $\dot{x}_{av}(t)$ for the current time t by summing the instantaneous velocity values in the time interval (t-T; T) and divide by the number N sum elements according to the formula:

$$\dot{x}_{av}(t) = \frac{1}{T}\int_{t-T}^{t} \dot{x}_i(t)dt \approx \frac{1}{N}\sum_{j=0}^{N} \dot{x}_{ij} \tag{4}$$

Step 3.

– Subtract from velocity $\dot{x}_i(t)$ of its average value $\dot{x}_{av}(t)$; $\dot{x}_c(t) = \dot{x}_i(t) - \dot{x}_{av}(t)$.

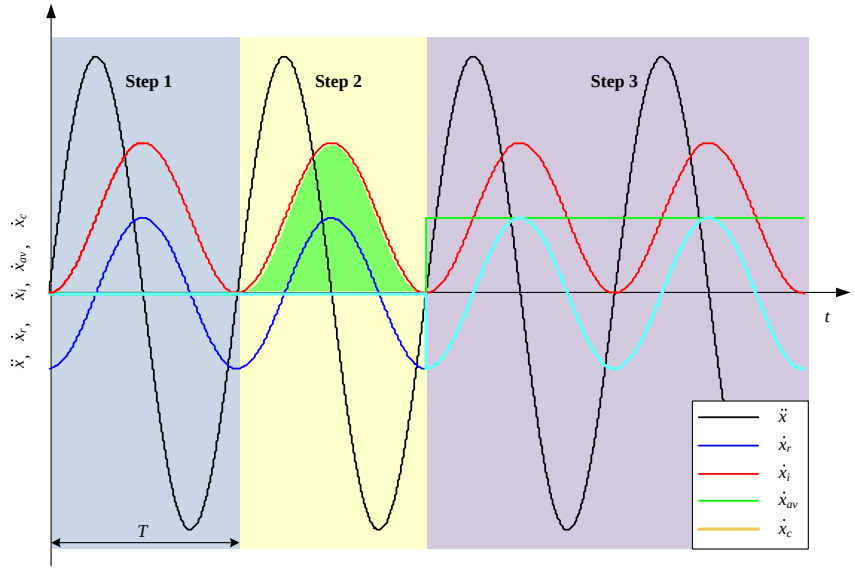

Fig. 6. Conversion of acceleration signal into velocity signal with drift removing method

The calculation of the average velocity $\dot{x}_{av}(t)$ first requires the period T of the acceleration $\ddot{x}(t)$ to be detected, and then the integer from the signal $\dot{x}_i(t)$ to be determined for the same period, which means that the correct value of the velocity signal $\dot{x}_c(t)$ is determined after at least 2T. Incorrect velocity values would cause the sky-hook algorithm to malfunction. Therefore, it was assumed that for a time of 1 s (which corresponds to two periods of a signal with a frequency of 2 Hz), the calculated velocities $\dot{x}$ and $\dot{z}$ take a value of 0. Thus, the set value of the current in the MR damper coil is given as ids = 0, and at this time it works in the passive mode (no power supply to the MR damper coil).

5. TEST RESULTS AND DICUSSION

Examination of the MR damper control system with EU was carried out in two stages. In the first stage, the correctness of the calculation of velocity signals $\dot{z}_c$ and $\dot{x}_c$ was checked based on measured acceleration signals $\ddot{z}$ and $\ddot{x}$ using MEMS accelerometers S1 and S2 (see Fig. 5). Figs. 7 and 8 show, respectively, the waveforms of reference velocities $\dot{z}_r$ and $\dot{x}_r$ (measured by a Polytec OFV-505 sensor with an OFV-5000 controller [32]) and calculated velocities $\dot{z}_c$ and $\dot{x}_c$ at a sine excitation with amplitude A = 3.5 mm and frequencies f: 3.3 Hz, 3.7 Hz, 5.5 Hz and 10 Hz.

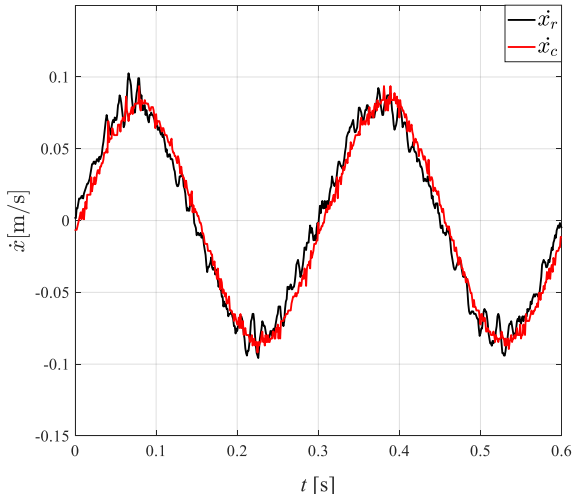

(a)

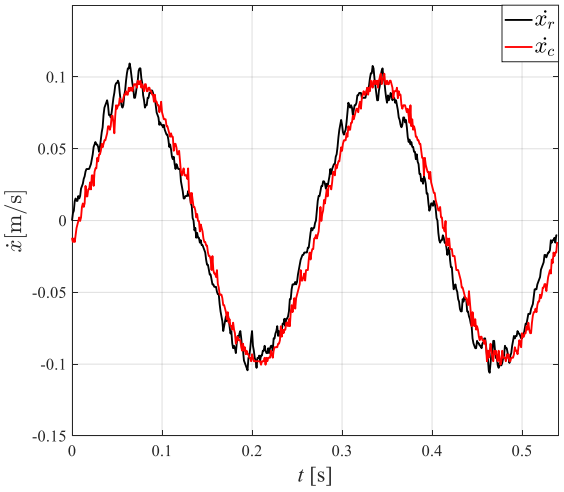

(b)

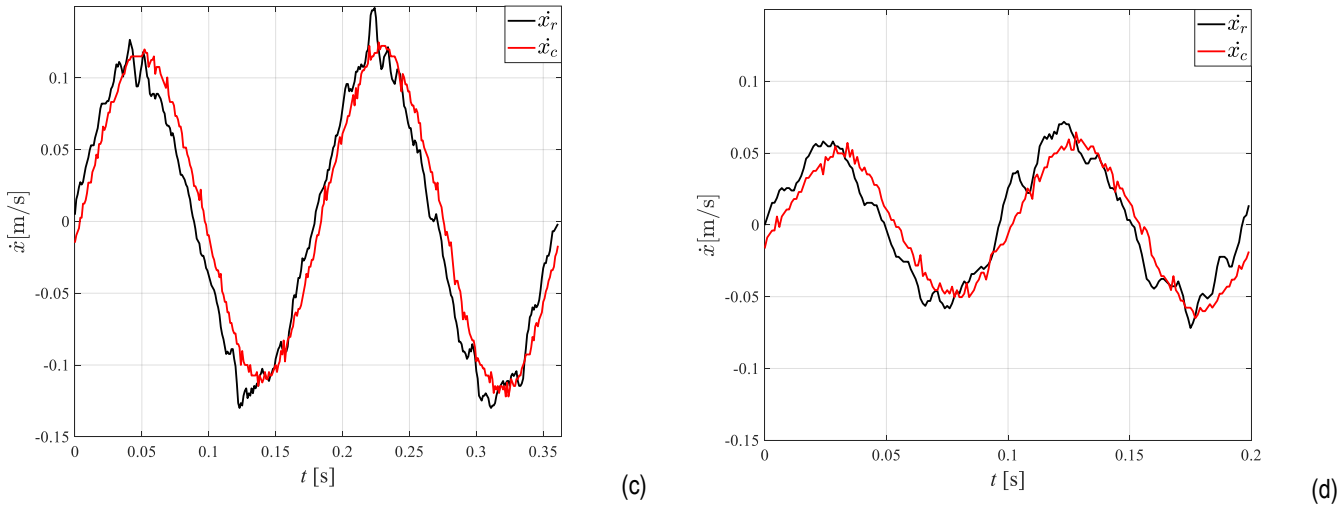

Fig. 7. Time patterns of velocities $\dot{x}_r$ and $\dot{x}_c$ at frequency f: (a) 3.3 Hz, (b) 3.7 Hz, (c) 5.5 Hz, (d) 10 Hz

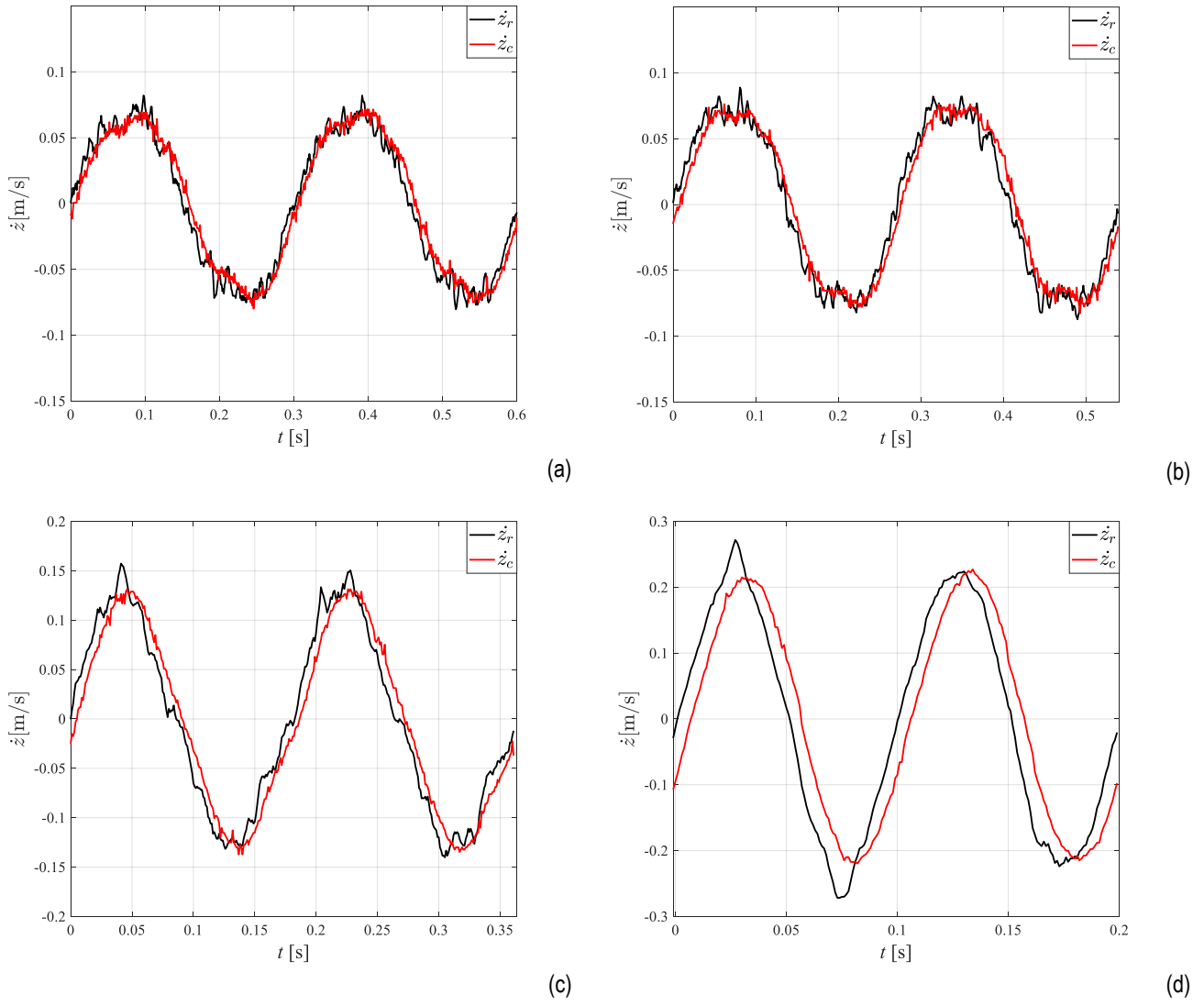

Fig. 8. Time patterns of velocities $\dot{z}_r$ and $\dot{z}_c$ at frequency f: (a) 3.3 Hz, (b) 3.7 Hz, (c) 5.5 Hz, (d) 10 Hz

As can be seen, the amplitude of the calculated velocities $\dot{z}_c$ and $\dot{x}_c$ corresponds to reference velocity amplitudes $\dot{z}_r$ and $\dot{x}_r$. The apparent time delay (due to signal conversion by the A/D μC converter and the required calculations, including numerical integration) is approx. 5 ms and does not depend on the frequency f. This delay also affects the time shift of the current ids calculated

DOI 10.2478/ama-2024-0020

by the sky-hook algorithm.

In the second stage, the control of the MR damper with vibration energy harvesting realised by the EU was tested in the test rig (Fig. 5). Tests were conducted with sine excitations with amplitude A = 3.5 mm and frequency f in the range (2, 10) Hz in increments of 0.1 Hz for the following cases:

- NS - no power supply to the MR damper control coil;
- DS - MR damper coil powered directly by harvester voltage uh;
- DR - MR damper coil powered with DC current uDC from the EU (the DU unit permanently connects the coil to the RB unit), the EU being powered by the harvester voltage uh;
- EEC - the current in the MR damper coil is controlled by the EU according to the implemented algorithm and energy from an external 5 V power supply is used;
- EHC - the current in the MR damper coil is controlled by the EU according to the implemented algorithm and only the energy recovered by the harvester is used.

The EEC case is a reference for the other cases and at the same time serves to demonstrate the correctness of the implementation of the sky-hook algorithm in the EU. Displacement transmissibility was used to evaluate the efficiency of MR damper control $T_{xz}(f)$ defined as follows:

$$T_{xz}(f) = \frac{\sqrt{\int_0^{\frac{1}{f}} x(t)^2 dt}}{\sqrt{\int_0^{\frac{1}{f}} z(t)^2 dt}} \tag{5}$$

Fig. 9 shows the relationship $T_{xz}(f)$ for all the above cases of power supply/control of the MR damper coil.

It should be noted that in the case of NS, the maximum value T_{xz} is achieved for frequency f = 3.8 Hz and is given as T_{xz} = 3.6. This frequency is equal to the frequency f_r, at which resonance occurs in the 1DOF system (lowest damping, i_d = 0). Direct powering of the MR damper coil by the harvester (DC case) reduces the vibration amplitude of the sprung mass at frequencies f < 4.8 Hz and increases it for higher frequencies when compared to the NS case. The same situation occurs with the DR case at frequencies f > 5.1 Hz. In the cases of DS and DR, the maximum values T_{xz} occur, respectively, at f = 4.2 Hz and f = 3.2 Hz and are 1.7 and 2.2. In order to eliminate this adverse phenomenon, the sky-hook algorithm was used to control the current in the MR damper coil. For the considered cases of powered/controlled MR damper, the lowest values T_{xz} in the frequency range (2, 10) Hz occur in the case of EEC (at frequency f = 4 Hz, maximum value T_{xz} is 1.25). In the EEC and EHC cases, at frequencies f > 5.5 Hz, the increase in the value T_{xz} does not exceed 5% compared to that in the case of NS. It should be noted that in the cases of EEC and EHC there are significant differences in the values T_{xz} in the frequency range (2.4, 4.4) Hz. The higher value T_{xz} in the case of EHC results from insufficient energy recovery.

Figs. 10–13 show the frequency characteristics of the effective voltage values (RMS values) U_h, currents I_h and I_d and power F_d.

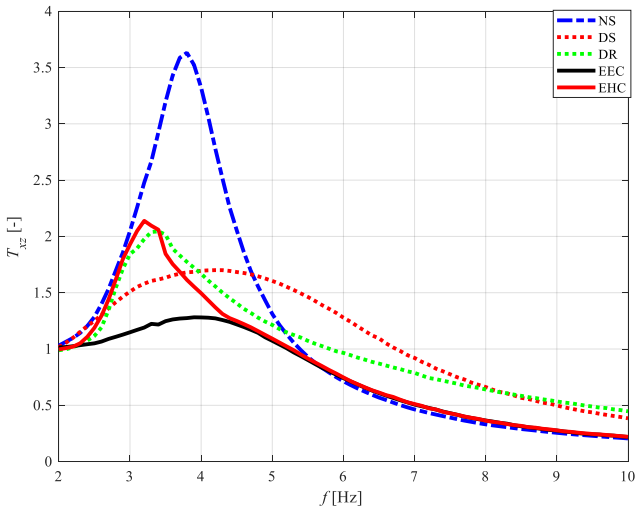

Fig. 9. Displacement transmissibility coefficients T_{xz}

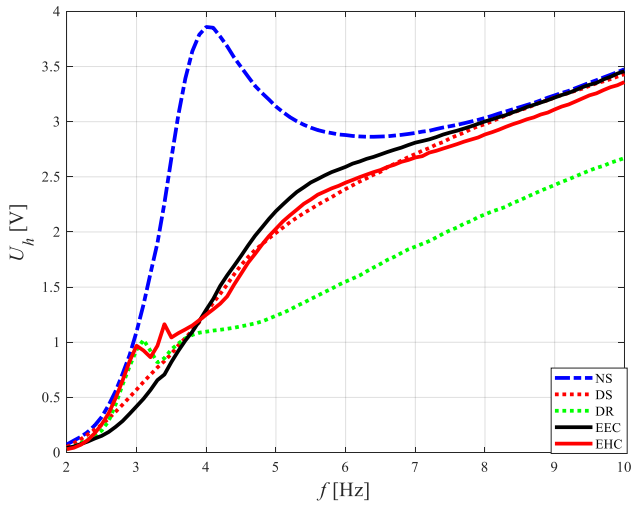

Fig. 10. Harvester coil voltage U_h vs. frequency f

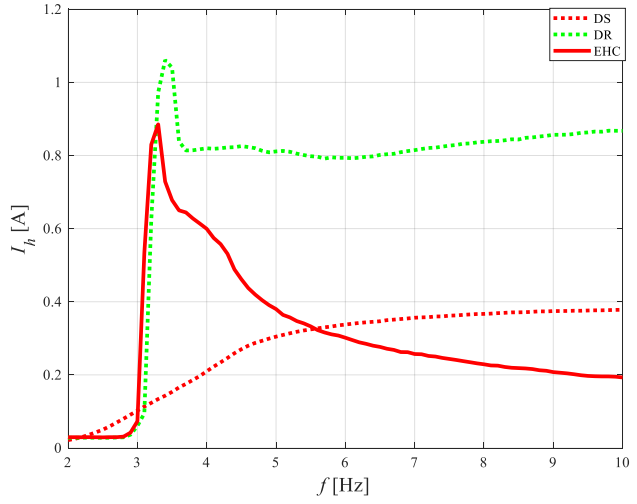

Fig. 11. Harvester coil current I_h vs. frequency f

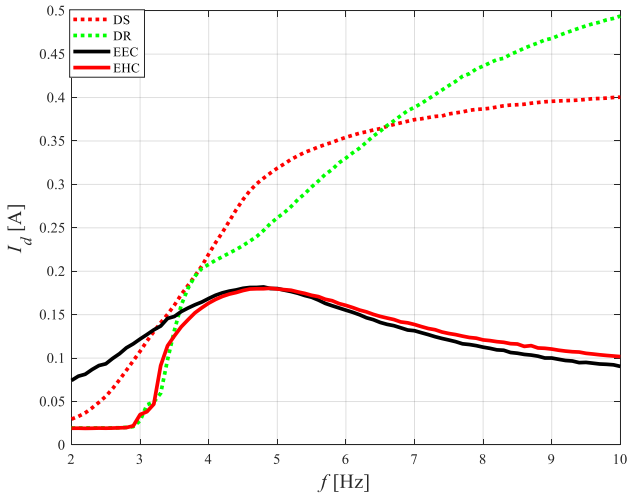

Fig. 12. MR damper coil current I_d vs. frequency f

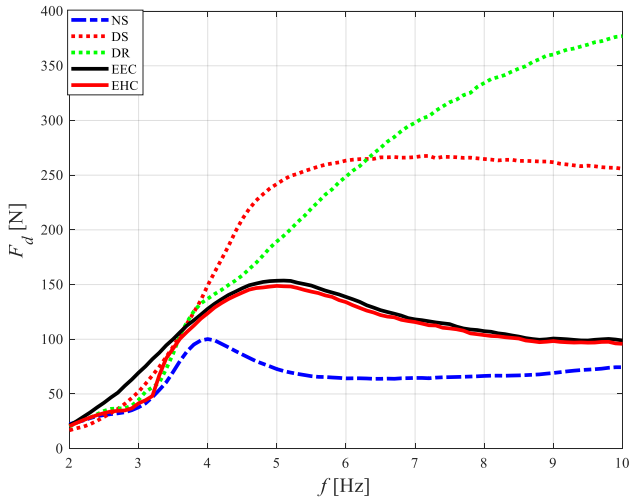

Fig. 13. MR damper force F_d vs. frequency f

Analysing the graphs in Fig. 10, it can be seen that the voltage U_h does not exceed 4 V, with the highest value occurring in the case of NS at a frequency of f = 4 Hz. The EU works stably when voltage U_h reaches at least 1.3 V (the EHC and DR cases at a frequency of f > 3.7 Hz). This results in less vibration damping compared to the EEC case at frequencies f < 4 Hz (Fig. 9). It is clearly seen that in the EHC and DR cases, current I_h = 0 (Fig. 11) and I_d = 0 (Fig. 12) at frequencies f < 3 Hz. A maximal value of I_h is achieved in the frequency range (3.1, 3.5) Hz, which is due to the inclusion of DC/DC converters in the IPS unit, which power the electrical circuits of the EU and accelerometers S1 and S2. The largest current consumption I_h occurs in the DR case at frequencies f > 4 Hz. The graphs in Figs. 12 and 13 show that at frequencies f > 5 Hz, the sky-hook algorithm results in a significant reduction in current I_d and the force F_d that depends on it (EEC and EHC cases) compared to DS and DR. Thanks to this value T_{xz}, in the case of EEC and EHC, it does not increase as in the case of DS and DR (Fig. 9).

The graphs in Fig. 14 confirm the correct operation of the sky-hook algorithm implemented in the EU when powered from an external power source. Instantaneous current value i_{ds} is calculated based on the measured velocity values $\dot{x}$ and $\dot{z}$ by an external measuring system, according to Eq. (1). The on–off regulator implemented in the EU facilitates achieving control of the instantaneous current value i_d in the MR damper coil. It should be emphasised that the μC calculates the set value i_{ds} of the current i_d also according to Eq. (1) using velocity signals $\dot{x}_c$ and $\dot{z}_c$ for this purpose, calculated from measured accelerations $\ddot{x}$ and $\ddot{z}$. The calculated time delays (Figs. 7 and 8) and the dynamic properties of the MR damper coil cause a current delay i_d relative to the current set value i_{ds} of about 8 ms (Fig. 14) regardless of frequency excitation f.

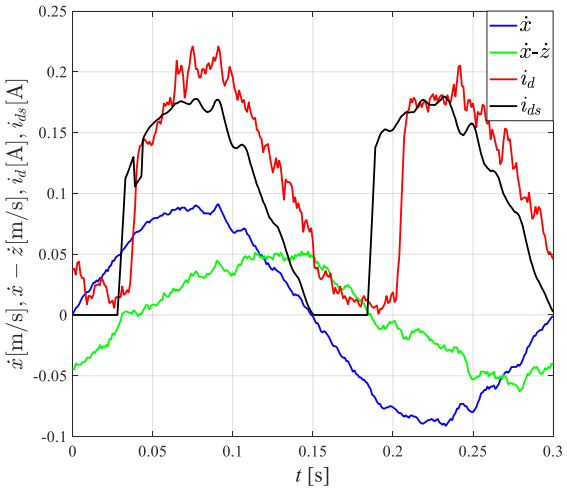

(a)

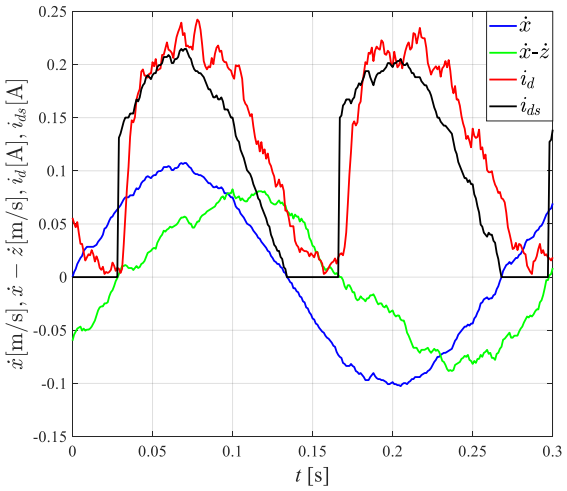

(b)

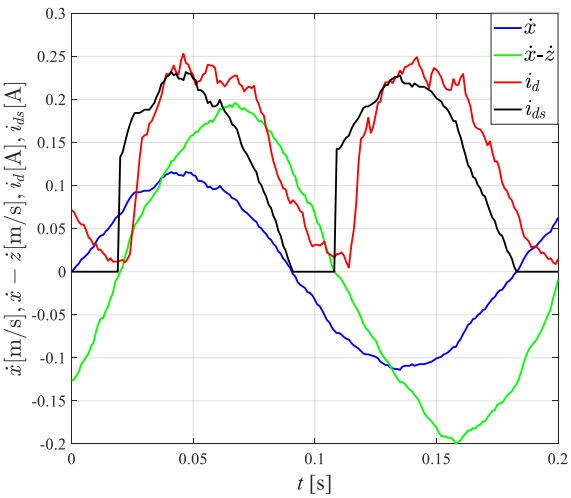

(c)

DOI 10.2478/ama-2024-0020

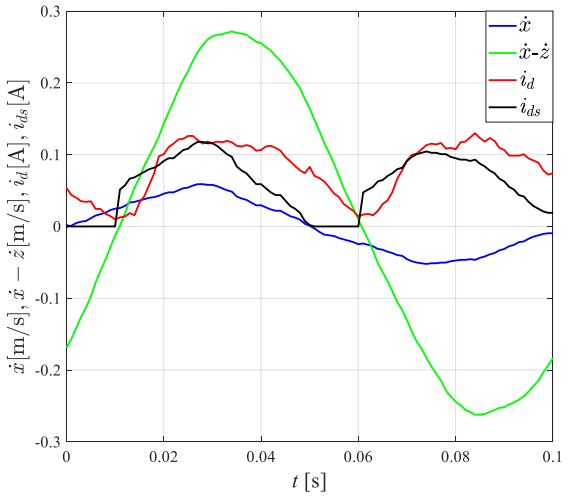

(d)

Fig. 14. Time patterns of sprung mass velocity $\dot{x}$, relative velocity $\dot{x}$ - $\dot{z}$, set current i_{ds}, coil current i_d at frequency f: (a) 3.3 Hz, (b) 3.7 Hz, (c) 5.5 Hz, (d) 10 Hz; external power

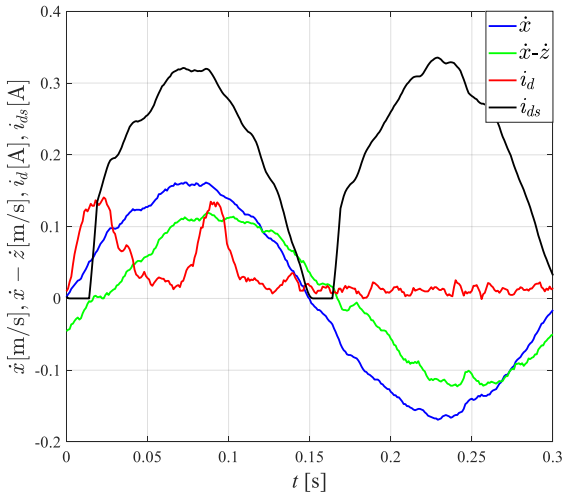

(a)

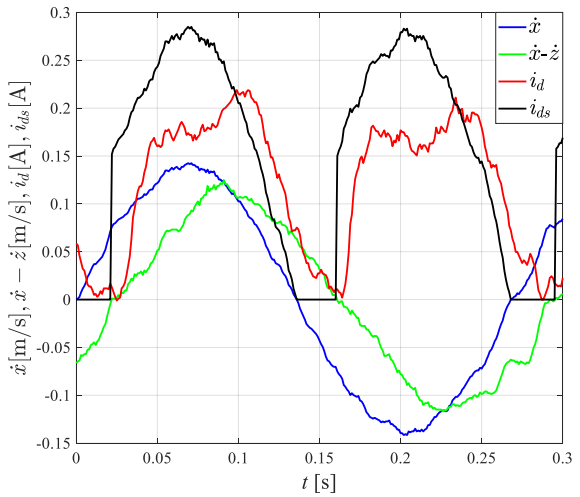

(b)

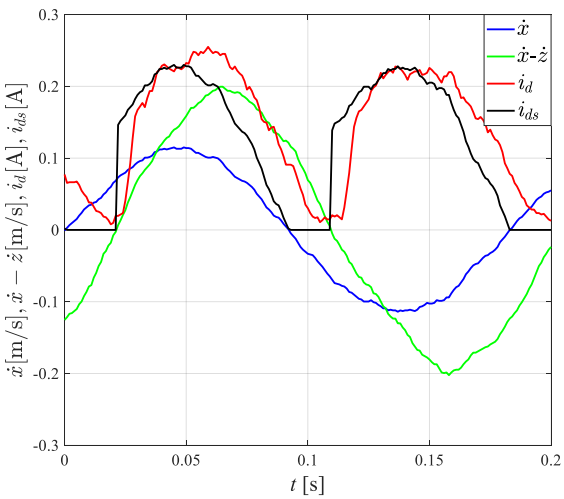

(c)

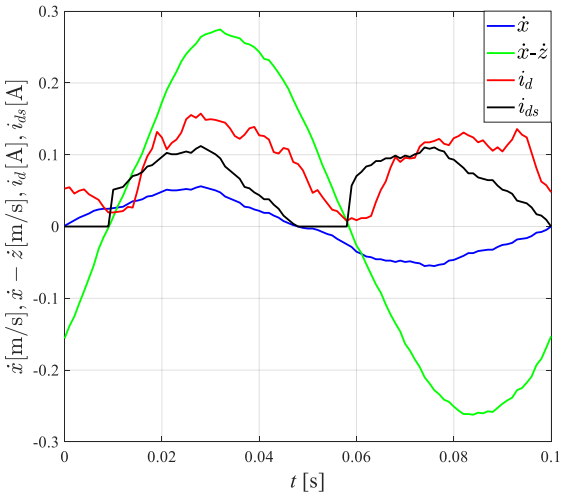

(d)

Fig. 15. Time patterns of sprung mass velocity $\dot{x}$, relative velocity $\dot{x}$ - $\dot{z}$, set current i_{ds}, coil current i_d at frequency f: (a) 3.3 Hz, (b) 3.7 Hz, (c) 5.5 Hz, (d) 10 Hz; energy harvesting

At frequencies f < 3.7 Hz, when the EU is powered by energy recovered from vibration, it can be seen that the current i_d takes less value than i_{ds}, which are required by the algorithm (Fig. 15a, b). This is due to the unstable operation of the EU at too low voltages U_h. The plots in Fig. 15c, d show the correct implementation of the algorithm in the system.

6. CONCLUSIONS AND OUTLOOK

The work presents the examination of the MR damper control system under harmonic kinematic excitations of low frequency range. The benefit of the proposed system is that it is powered exclusively by energy extracted from a vibrating structure and processed through the developed EU. It was demonstrated that the system enables effective control of the MR damper in a mechanical system with one-degree-of freedom.

The test results lead us to the following detailed conclusions:

– at resonance frequency f_r, an EU powered from an external energy source (EEC case) or energy recovered from vibrations (EHC case) causes 2.8-fold and 1.7-fold decreases in

the amplitude of the sprung mass, respectively;

- at frequency excitation f > 5.5 Hz in the EEC and EHC cases, there is an increase in T_{xz} by 5% compared to the NS case (no power supply to the MR damper coil), while in the DS and DR cases the value T_{xz} increases 2-fold;
- the correctness of the implementation of the sky-hook algorithm and, as a consequence, the control of the MR damper coil are confirmed by the following: $T_{xz}(f)$ and electricity id(t) in the EEC and EHC cases;
- an EU powered by energy harvested from vibrations works stably when the harvester voltage uh exceeds 1.3 V, which occurs at a frequency excitation of f > 3.7 Hz;
- in the frequency range (2.4, 4.4) Hz, higher values of $T_{xz}(f)$ occur in the EHC case (power supply from vibration recovered energy) than in the EEC case (power supply from an external voltage source), which is due to the insufficient amount of energy recovered.
- Ongoing research is focussed on:
- eliminating of the acceleration sensor S1 from the control system, using the harvester output voltage u_h for this purpose converted to relative velocity;
- testing methods of achieving conversion of acceleration observed with non-harmonic types of excitations into velocity;
- testing other MR damper control algorithms;
- using the harvested energy storage (when the harvester is not able to generate enough energy) to maintain the voltage to allow the EU to function properly.

REFERENCES

1. Priya S, Inman DJ, editors. Energy Harvesting Technologies. Boston, MA: Springer US. 2009. https://doi.org/10.1007/978-0-387-76464-1
2. Harb A. Energy harvesting: State-of-the-art. Renewable Energy. 2011 Oct 1;36(10):2641–54. http://dx.doi.org/10.1016/j.renene.2010.06.014
3. Siang J, Lim M H., Salman Leong M. Review of vibration-based energy harvesting technology: Mechanism and architectural approach. International Journal of Energy Research. 2018 Jan 18; 42(5):1866–93. https://doi.org/10.1002/er.3986
4. Wei C, Jing X. A comprehensive review on vibration energy harvesting: Modelling and realization. Renewable and Sustainable Energy Reviews. 2017 Jul 1;74:1–18. https://doi.org/10.1016/j.rser.2017.01.073
5. Sun R, Zhou S, Cheng L. Ultra-low frequency vibration energy harvesting: Mechanisms, enhancement techniques, and scaling laws. Energy Conversion and Management. 2023 Jan 15;276:116585. https://doi.org/10.1016/j.enconman.2022.116585
6. Brennan MJ, Tang B, Pechoto G, Lopes V. An investigation into the simultaneous use of a resonator as an energy harvester and a vibration absorber. Journal of Sound and Vibration. 2014 Feb 1;333(5):1331–43. https://doi.org/10.1016/j.jsv.2013.10.035
7. Toyabur RM, Salauddin M, Cho H, Park JY. A multimodal hybrid energy harvester based on piezoelectric-electromagnetic mechanisms for low-frequency ambient vibrations. Energy Conversion and Management. 2018 Jul 15;168:454–66. https://doi.org/10.1016/j.enconman.2018.05.018
8. Wang X, Liang X, Wei H. A study of electromagnetic vibration energy harvesters with different interface circuits. Mechanical Systems and Signal Processing. 2015 Jun 1;58–59:376–98. https://doi.org/10.1016/j.ymssp.2014.10.004
9. Wang X, Liang X, Hao Z, Du H, Zhang N, Qian M. Comparison of electromagnetic and piezoelectric vibration energy harvesters with different interface circuits. Mechanical Systems and Signal Processing. 2016 May 1;72–73:906–24. https://doi.org/10.1016/j.ymssp.2015.10.016
10. Shen W, Zhu S, Xu Y. An experimental study on self-powered vibration control and monitoring system using electromagnetic TMD and wireless sensors. Sensors and Actuators A: Physical. 2012 Jun 1;180:166–76. https://doi.org/10.1016/j.sna.2012.04.011
11. Cai Q, Zhu S. Enhancing the performance of electromagnetic damper cum energy harvester using microcontroller: Concept and experiment validation. Mechanical Systems and Signal Processing. 2019 Dec 1;134:106339-9. https://doi.org/10.1016/j.ymssp.2019.106339
12. Sapiński B, Orkisz P, Jastrzębski Ł. Experimental Analysis of Power Flows in the Regenerative Vibration Reduction System with a Magnetorheological Damper. Energies. 2021 Feb 6;14(4):848. http://dx.doi.org/10.3390/en14040848
13. Jastrzębski Ł, Sapiński B. Magnetorheological Self-Powered Vibration Reduction System with Current Cut-Off: Experimental Investigation. Acta Mechanica et Automatica. 2018 Jun 1;12(2):96–100. https://doi.org/10.2478/ama-2018-0015
14. Sapiński B. An experimental electromagnetic induction device for a magnetorheological damper. Journal of Theoretical and Applied Mechanics. 2008;46(4):933–47.
15. Sapiński B. Vibration power generator for a linear MR damper. Smart Materials and Structures. 2010 Aug 6;19(10):105012. http://doi.org/10.1088/0964-1726/19/10/105012
16. Kozieł A, Jastrzębski Ł, Sapiński B. Advanced Prototype of an Electrical Control Unit for an MR Damper Powered by Energy Harvested from Vibrations. Energies. 2022 Jun 21;15(13):4537. https://doi.org/10.3390/en15134537
17. Texas Instruments, Technical documentation available online: https://www.ti.com/ (accessed on Jun 30, 2023).
18. STMicroelectronics, Technical documentation available online: http://www.st.com/ (accessed on Jun 30, 2023).
19. MR Damper, RD-8040-1, Technical documentation available online: http://www.lordfulfillment.com/upload/DS7016.pdf (accessed on Jun 30, 2023).
20. Gołdasz J, Sapiński B, Jastrzębski Ł, Kubik M. Dual Hysteresis Model of MR Dampers. Frontiers in Materials. 2020 Oct 6; 7:236. https://doi.org/10.3389/fmats.2020.00236
21. Choi SB, Li W, Yu M, Du H, Fu J, Do PX. State of the art of control schemes for smart systems featuring magneto-rheological materials. Smart Materials and Structures 2016 Mar 14;25(4):043001. https://doi.org/10.1088/0964-1726/25/4/043001
22. Karnopp D, Crosby MJ, Harwood RA. Vibration Control Using Semi-Active Force Generators. Journal of Engineering for Industry. 1974 May 1;96(2):619–26. https://doi.org/10.1115/1.3438373
23. Sapiński B, Rosół M. MR damper performance for shock isolation. Journal of Theoretical and Applied Mechanics. 2007;45(1):133–45.
24. Analog Devices, Technical documentation available online: https://www.analog.com/en/index.html (accessed on Jun 30, 2023).
25. Thenozhi S, Yu W, Garrido R. A novel numerical integrator for velocity and position estimation. Transactions of the Institute of Measurement and Control. 2013 Aug 1;35(6):824–33. https://doi.org/10.1177/0142331213476987
26. Arias-Lara D, De-la-Colina J. Assessment of methodologies to estimate displacements from measured acceleration records. Measurement. 2018 Jan 1;114:261–73. https://doi.org/10.1016/j.measurement.2017.09.019
27. Hamming RW. Digital filters (3rd ed.). GBR: Prentice Hall International (UK) Ltd.; 1989. 284 p.
28. Guo R, Ye S, Ji Y. Optimization Acceleration Integral Method Based on Power Spectrum Estimation. MATEC Web Conf. 2018;176:03012. https://doi.org/10.1051/matecconf/201817603012

29. Han H, Park M, Park S, Kim J, Baek Y. Experimental Verification of Methods for Converting Acceleration Data in High-Rise Buildings into Displacement Data by Shaking Table Test. Applied Sciences 2019 Apr 21;9(8):1653-3. https://doi.org/10.3390/app9081653.
30. Park KT, Kim SH, Park HS, Lee KW. The determination of bridge displacement using measured acceleration. Engineering Structures. 2005 Feb 1;27(3):371–8. https://doi.org/10.1016/j.engstruct.2004.10.013
31. Yang Y, Zhao Y, Kang D. Integration on acceleration signals by adjusting with envelopes. Journal of Measurements in Engineering. 2016 Jun 30;4(2):117–21.
32. Polytec, Technical documentation available online: https://www.polytec.com (accessed on Jun 30, 2023).

This research was funded by the AGH University of Krakow within the scope of the research program No. 16.16.130.942.

Łukasz Jastrzębski: https://orcid.org/0000-0002-2210-835X

Bogdan Sapiński: https://orcid.org/0000-0001-6952-8303